


Carrier Drift Control of Spin Currents in Graphene-Based Spin-Current Demultiplexers

J. Ingla-Aynés,^{*} A. A. Kaverzin, and B.J. van Wees

Physics of Nanodevices, Zernike Institute for Advanced Materials, University of Groningen, 9747 AG Groningen, Netherlands

 (Received 8 June 2018; revised manuscript received 19 August 2018; published 31 October 2018)

Electrical control of spin transport is promising for achieving new device functionalities. Here we calculate the propagation of spin currents in a graphene-based spin-current demultiplexer under the effect of drift currents. We show that, using spin- and charge-transport parameters already obtained in experiments, the spin currents can be guided in a controlled way. In particular, spin-current selectivities up to 10^2 can be achieved for measurements over a distance of $10\ \mu\text{m}$ under a moderate drift current density of $20\ \mu\text{A}/\mu\text{m}$, meaning that the spin current in the arm that is *off* is only 1% of the current in the arm that is *on*. To illustrate the versatility of this approach, we show similar efficiencies in a device with four outputs and the possibility of multiplexer operation using spin drift. Finally, we explain how the effect can be optimized in graphene and two-dimensional semiconductors.

DOI: [10.1103/PhysRevApplied.10.044073](https://doi.org/10.1103/PhysRevApplied.10.044073)

I. INTRODUCTION

The ability to manipulate spin currents by electrical means is a major requirement to achieve functional spintronic devices [1]. For this purpose, graphene is an ideal candidate as a transport medium thanks to its superior spin- and charge-transport properties [2–6]. These properties have allowed room-temperature spin relaxation lengths up to $30\ \mu\text{m}$ in an experiment where spin transport is diffusive [6] and up to $90\ \mu\text{m}$ when carrier drift was additionally induced in the channel [7]. Moreover, enhancements in the spin-injection and detection efficiencies [8–10] show the possibility to create unprecedentedly large spin accumulations in graphene, resulting in larger signals useful for future spintronic operations.

It has been shown that one can perform logic operations using spins in graphene in the diffusive regime. In particular, the interplay between the spin-injection efficiencies of different contacts can be used to perform logic XOR operations [11]. The introduction of transition-metal dichalcogenides (TMDs) also allows control of the spin signals in graphene-based spintronic devices. The tunability of the TMD resistance allows efficient control of the spin absorption in such structures, resulting in on:off ratios of up to 60 [12,13]. Another means of controlling spin currents was demonstrated in Y-shaped graphene devices via the manipulation of carrier densities in the different arms individually [14]. This approach leads to spin guiding thanks to the change in spin lifetime and resistivity of graphene with the carrier density. On:off ratios for spin

currents of up to 7 were obtained under the assumption that the spin relaxation time in the channel decreases when the resistivity increases, a condition achieved experimentally only for bilayer graphene on SiO_2 at temperatures equal to or lower than 50 K [15–17].

The spin signals achieved by diffusive transport are limited by the long diffusion times, which increase with the square of the distance [1]. However, a charge current can significantly influence the spin propagation. The average velocity of spin carriers is much greater (lower) when transport occurs in the direction of (against) the drift velocity (v_d). This allows efficient control of the spin relaxation length with use of charge currents [7,18] without affecting the spin lifetime in the system. In addition, v_d is inversely proportional to the carrier density. This brings a new mechanism to control the magnitude and sign of v_d . The tunability of spin transport with drift enables new device functionalities, such as demultiplexers, which are devices that route the input signal to an output that is controlled by the select line [19]. Demultiplexers have applications ranging from analog switches in high-frequency transmission lines to decoders in digital electronics [20,21], and combination of spin currents with multiplexer operations could allow *in situ* memory capabilities, enabling new functionalities [22,23].

Here we show that, by applying drift currents in a Y-shaped geometry, the spin currents can be controlled in an extremely efficient way, realizing the demultiplexer functionality. Our calculations using the drift-diffusion equation show that one can achieve spin-current selectivities $I_{\text{top}}/I_{\text{bot}}$ (where I_{top} is the spin current in the top arm and I_{bot} is the spin current in the bottom arm

^{*}j.ingla.aynes@rug.nl

in Fig. 1) as high as 10^3 for drift-current densities of $100 \mu\text{A}/\mu\text{m}$ when measurements are made close to the bifurcation. At a distance $L = 10 \mu\text{m}$ from the bifurcation, the selectivities increase to 10^6 , and are as high as 10^2 for drift-current densities of $20 \mu\text{A}/\mu\text{m}$. Moreover, we use the same model for a geometry constituting of two Y-shaped graphene channels connected to the output of another Y-shaped graphene channel, and obtain similar performance of 10^2 for drift currents of $25 \mu\text{A}/\mu\text{m}$. We also explain how the effect of drift can be used to achieve multiplexer operation. From these considerations, we conclude that the introduction of drift leads to several advantages when compared with the diffusive case. These advantages include a significant enhancement in the speed of operations, a significant increase of the on:off ratio, and higher spin currents due to the increase of the spin relaxation lengths induced by the drift. On the other hand, the introduction of drift to spin logic also causes extra power consumption induced by the drift currents. We argue that

this can be greatly reduced by replacing graphene with a semiconducting two-dimensional (2D) material.

Moreover, the technique described here can also be used in combination with other implementations, such as the XOR operation described in Ref. [11], that can be added to our geometry to combine multiplexer with logic operations.

II. THE MODEL

To determine the spin currents and spin accumulations in the different geometries studied here under the effect of drift, we use the drift-diffusion equation [24].

Since in most graphene-based spin-valve devices the contacts inject spins homogeneously over the channel width, we reduce the spin propagation to a one-dimensional problem. Also, we assume that the channel width (W_s) is much longer than the mean free path. This condition is commonly achieved for all graphene spintronic devices studied at room temperature for $W_s = 1 \mu\text{m}$ (the mean free path is $0.16 \mu\text{m}$ in our case). This condition makes our results independent of the exact geometry of the bifurcation. We also assume that the contacts are not invasive; this condition is achieved when the contact resistances are much higher than the channel resistance [25].

When a charge current I_d is applied to a nonmagnetic [26] channel to induce drift, the spin current propagating in the channel is [27]

$$I_s = \frac{W_s}{eR_{\text{sq}}} \left(-\frac{d\mu_s}{dx} + \frac{v_d}{D_s} \mu_s \right). \quad (1)$$

Here D_s is the spin-diffusion coefficient, R_{sq} is the square resistance, μ_s is the spin accumulation, and e is the electron charge. The drift velocity is defined as $v_d = \mu I_d R_{\text{sq}} / W_s = I_d / (enW_s)$, where n is the carrier density and μ is the electron mobility. The first term in Eq. (1) describes the spin diffusion and the second one describes the spin current induced by the pulling of the spin accumulation induced by the drift.

In the channel, μ_s follows the drift-diffusion equation [24]:

$$D_s \frac{d^2 \mu_s}{dx^2} + v_d \frac{d\mu_s}{dx} - \frac{\mu_s}{\tau_s} = 0, \quad (2)$$

where τ_s is the spin lifetime. This equation has solutions of the form $\mu_s = A \exp(x/\lambda_+) + B \exp(-x/\lambda_-)$, where the coefficients A and B are determined by both the device geometry and the spin relaxation lengths, which are

$$\lambda_{\pm}^{-1} = \pm \frac{v_d}{2D_s} + \sqrt{\left(\frac{v_d}{2D_s} \right)^2 + \frac{1}{\lambda^2}}, \quad (3)$$

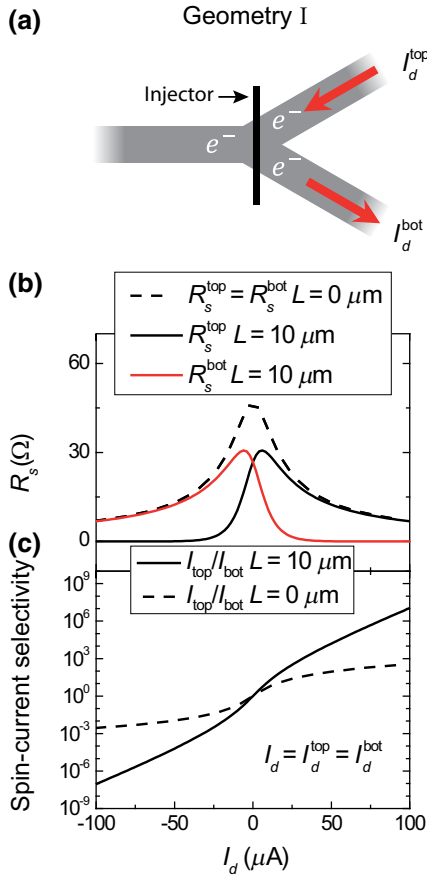


FIG. 1. (a) Device geometry I. The red arrows represent the charge-current direction for positive I_d . The carriers are electrons in all three arms, which are assumed to be infinitely long. (b) R_s versus I_d in the top and bottom arms and close to the bifurcation and at a distance of $10 \mu\text{m}$. (c) Spin-current selectivity calculated both close to the bifurcation ($L = 0$) and at $L = 10 \mu\text{m}$.

where $\lambda = \sqrt{D_s \tau_s}$ is the spin-diffusion length in the channel. λ_+ and λ_- are the so-called upstream and downstream spin relaxation lengths. They describe spin transport opposed to and along the direction of the drift velocity, respectively. Their difference provides an asymmetry in the spin propagation, which is the source of spin-current selectivity in our calculations.

We use the solutions of Eq. (2) to describe the spin accumulation in the different parts of the sample. Because the drift currents and/or carrier densities are different in the different parts of the sample, the unknown coefficients are obtained with use of the following boundary conditions by taking into account the device geometry: μ_s is zero infinitely far away from the injector and it is continuous in the entire device, including the boundaries between the different regions. The spin current I_s is conserved at the different junctions apart from the injection point. The spin injector is a ferromagnetic electrode placed at the bifurcation point and it induces a discontinuity in the spin current of $P_i I_{\text{inj}}/e$, where P_i is the spin polarization of the injector and I_{inj} is the charge current applied to the injector electrode. For simplicity, the additional electrodes that are used to induce drift are placed further away from the bifurcation points than the relevant spin relaxation length and, therefore, are not considered to be spin injectors irrespective of the constituting materials. Under these conditions, we are able to obtain the spin currents and nonlocal resistances $R_s = V_s/I_{\text{inj}} = \mu_s P_d/(e I_{\text{inj}})$ (where $V_s = \mu_s P_d/e$ is the voltage drop caused by the spin accumulation at the detecting ferromagnetic electrode, which has spin polarization P_d) in the reported device geometries [25,28].

Because of the inverse dependence between v_d and n , v_d theoretically diverges at the neutrality point. However, thermal broadening [29,30] limits the minimal electron and hole densities to a value of $n_{\text{th}}^e = n_{\text{th}}^h = \pi/12[k_B T/(\hbar v_f)]^2 = 4 \times 10^{14} \text{ m}^{-2}$ at room temperature. In a system with equal amounts of electrons and holes, no drift is present since the drift velocities for electrons and holes are opposite. Thus, an imbalance between the electron and hole densities is required to achieve a nonzero average drift velocity. This condition increases the minimal carrier density, which is optimal for spin drift and, therefore, limits the drift velocity v_d that can be reached experimentally. For all the calculations reported here, we use transport parameters that were obtained experimentally in monolayer graphene [6] near the charge-neutrality point. They are given in Table I. In our case, the optimal carrier density is $8 \times 10^{15} \text{ m}^{-2}$ and, for a drift-current density of $100 \mu\text{A}/\mu\text{m}$, gives a drift velocity $v_d = 8 \times 10^4 \text{ m/s}$. This value is still 1 order of magnitude smaller than the maximum drift velocity achieved for boron nitride-encapsulated graphene, which is around $0.55 \times 10^6 \text{ m/s}$ at room temperature for a carrier density of about $9 \times 10^{15} \text{ m}^{-2}$ [31,32].

TABLE I. Spin-, charge-transport parameters, contact spin polarizations estimated from Ref. [6] and channel width. For simplicity we assume that the system is electron-hole symmetric and the sign of the drift velocity changes for hole transport.

μ ($\text{m}^2/\text{V s}$)	R_{sq} (Ω)	n (m^{-2})	τ_s (ns)	D_s (m^2/s)	$P_i = P_d$	W_s (μm)
1	800	8×10^{15}	4	0.08	0.1	1

III. RESULTS

A. Geometry I

We start the discussion of our results obtained for the Y-shaped device geometry, where the spin injector is placed at the bifurcation point. For geometry I, the three arms have the same transport parameters. The spins are guided by application of opposite drift currents in the top and bottom arms, as shown in Fig. 1, and this generates a spin signal R_s^{top} at the top arm and a spin signal R_s^{bot} at the bottom arm. In the left arm there is no net charge current and the propagation of spins is determined by diffusion. As we can see in Fig. 1(b), when a drift current is applied, R_s close to the bifurcation point decreases. This is because the spins are pulled away from the injector toward the top or bottom arm, reducing the spin accumulation. At $L = 0$, we observe that when the applied drift current is $100 \mu\text{A}$, $I_{\text{top}}/I_{\text{bot}}$ is as high as 10^3 . This implies that 99.9% of the spins are propagating along the direction of the drift velocity and only 0.1% of them propagate to the opposite arm. Looking at the spin signal $10 \mu\text{m}$ from the bifurcation, we see that the nonlocal resistance in the top arm differs from that in the bottom arm. This difference develops very rapidly with the applied drift due to both the exponential decay of the spin current with distance and the difference between upstream and downstream spin relaxation lengths. For example, for $I_d = 100 \mu\text{A}$, the spin-current selectivities are as high as 10^6 with $\lambda_- = 340 \mu\text{m}$ and $\lambda_+ = 0.97 \mu\text{m}$. Both R_s^{top} and R_s^{bot} at $L = 10 \mu\text{m}$ decrease for drift currents higher than $\pm 6 \mu\text{A}$. This is because, for infinitely long arms, the drift spreads the spins over a large distance λ_- . Since the injected spin current is constant, this results in reduction of the spin accumulation close to the injector. This effect can be reduced by application of the drift current over a finite length of the channel [27].

In real-device applications, the power consumption has to be kept minimal, and to achieve this we determine the device performance for lower drift currents. At $I_d = 20 \mu\text{A}$, a current selectivity of 10^2 is achieved. We consider this value to be enough for basic operations. It is also worth noting that, when a drift current of $100 \mu\text{A}$ is applied, 4.8% of the spin current is still propagating to the left arm, and the proportion increases to 20% when $I_d = 20 \mu\text{A}$.

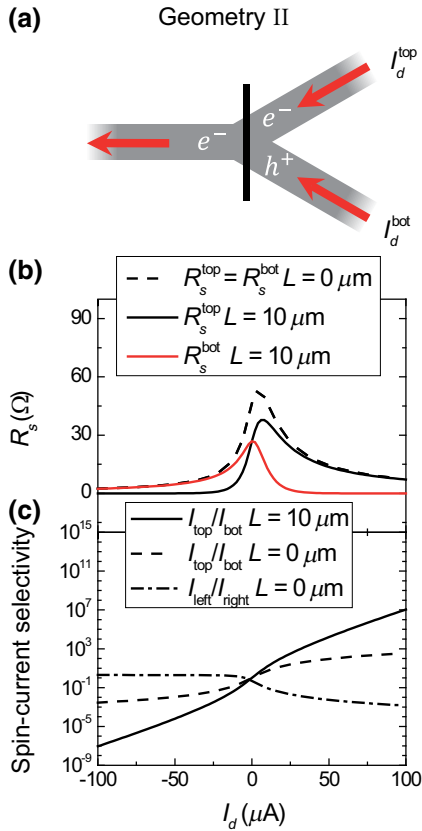


FIG. 2. (a) Device geometry II. The red arrows represent the charge-current direction for positive I_d . The direction of the drift velocity for electrons is opposite to the charge-current direction. The carriers are holes in the bottom arm and electrons in the other arms. All the arms are assumed to be infinitely long. (b) R_s versus I_d in the top and bottom arms and at the bifurcation and at a distance of $10 \mu\text{m}$. (c) Spin-current selectivity calculated both at the bifurcation and at a distance of $10 \mu\text{m}$.

B. Geometry II

As mentioned in the previous section, $I_{\text{left}}/I_{\text{right}}$, which is defined as the spin current propagating to the left arm I_{left} normalized by $I_{\text{right}} = I_{\text{top}} + I_{\text{bot}}$, is determined by diffusion in geometry I and it can be reduced by application of a net drift current in the left arm. This is achieved by change of the carrier type of either the top arm or the bottom arm depending on the selected output. When one changes the carriers from electrons to holes, the direction of the drift velocity reverses. This allows us to apply the drift current in both the top arm and bottom arm in the same direction ($I_d^{\text{top}} = I_d^{\text{bot}} = I_d$), while the drift velocities are opposite ($v_d^{\text{top}} = -v_d^{\text{bot}}$). In this case, the drift current in the left arm is nonzero and is equal to $2 \times I_d$. As shown in Fig. 2(b), R_s at $L = 0$ is no longer symmetric with respect to I_d . This is caused by the spin drift in the left arm, which blocks spin propagation to the left at positive drift currents but promotes spin propagation in this arm when I_d is negative.

TABLE II. Truth table for the two-leg demultiplexer operation of geometry II for positive I_d (Fig. 2).

V_{gL}	V_{gT}	V_{gB}	I_{top}	I_{bot}
1	1	0	1	0
1	0	1	0	1

As a consequence, we observe that the most-efficient operation of this device (maximum $I_{\text{top}}/I_{\text{bot}}$ and minimum $I_{\text{left}}/I_{\text{right}}$) occurs when the drift current is positive [drift currents in the direction of the red arrows in Fig. 2(a)]. The output terminal, where the current is directed, can be controlled by change of the carrier densities in the top and bottom arms while the left arm is kept at the same density and positive drift currents are applied [in the direction of the red arrows in Fig. 2(a)]. The spin-current selectivities in the top and bottom arms are the same as for geometry I due to electron-hole symmetry. The difference is that the spin current propagating to the left arm is kept minimal. In particular, when $I_d = 100 \mu\text{A}$, only 0.14% of the injected spin currents propagate into this arm, and the proportion is as low as 3% for $I_d = 20 \mu\text{A}$, confirming the feasibility of device operation with moderate drift currents.

C. Demultiplexing operation

As shown above, the most-efficient way of controlling the spin-demultiplexing operation is by the carrier type (density). To describe the practical operation of device geometry II, we construct a truth table (Table II) by defining the inputs as the gate voltages that have to be applied to each separate arm to control the densities. We call V_{gL} , V_{gT} , and V_{gB} the left-, top-, and bottom-arm gates, respectively, and define them as “0” when the carriers in the channel are holes and “1” when they are electrons.

D. Geometry III

Having understood the effect of drift in single Y-shaped graphene devices, we are interested in the operation of graphene channels with several Y-shaped devices connected in series for more-complex device functionality.

For this purpose, we design a device geometry that is made out of two Y-shaped graphene channels that are connected to the outputs of the first Y-shaped graphene channel. The distance between the bifurcation point where the spin injector is placed and the bifurcation point of the other two channels is $5 \mu\text{m}$ [Fig. 3(a)]. Using the model described above, we calculate the spin accumulations and spin currents required to understand the performance of these devices. The results are shown in Fig. 3 for a homogeneous device with the parameters shown in Table I. In this case, the nonlocal resistance also decreases for high drift currents. The spin-current selectivity between arms 1 and 2 (I_1/I_2) is lower than between arms 1 and 3 (I_1/I_3).

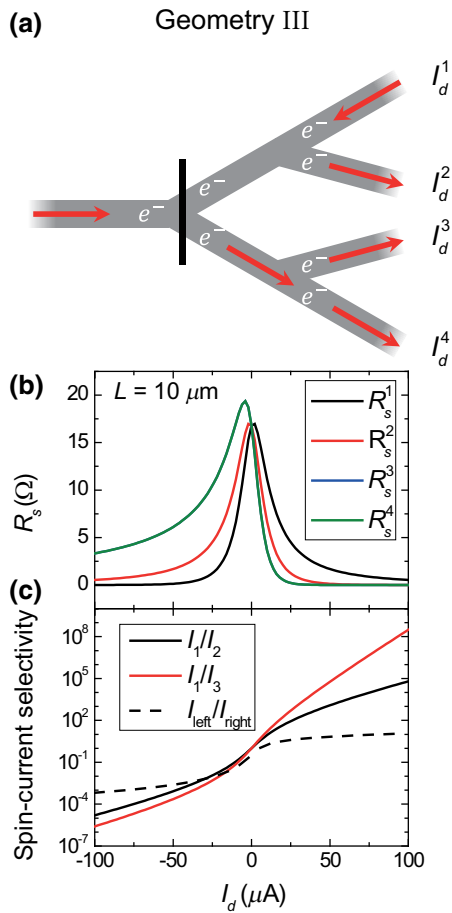


FIG. 3. (a) Device geometry III, with the spin currents propagating to output 1 for positive I_d in the direction of the red arrows. The drift velocity for holes is in the same direction as the drift current. The carriers are electrons in all the arms, the top and bottom bifurcations are at a distance of $x_1 = 5 \mu\text{m}$ from the spin injector, the detectors are at $L = 10 \mu\text{m}$, and the arms are assumed to be infinitely long. (b) R_s versus I_d in arms 1–4 at L . R_s^3 and R_s^4 are identical over all the range. (c) Spin-current selectivity between arm 1 and arm 2 and between arm 1 and arm 3 calculated at $x = L$, and $I_{\text{left}}/I_{\text{right}}$ calculated at $x = 0$.

This can be explained by taking into account that arms 1 and 2 share a $5\text{-}\mu\text{m}$ -long channel where there is no drift current, whereas the drift in the bottom arm is $2 \times I_d$ and opposes spin propagation. When looking at the spin current propagating in the left arm, we see that it increases for positive drift currents. This is because the drift current in this arm is $2 \times I_d$ and it promotes spin propagation away from the injector at positive drift currents. This is not efficient since at $I_d = 100 \mu\text{A}$ the spin current propagating toward the left is 11 times higher than the one propagating toward the right and, hence, less than 10% of the injected spins contribute to the operation.

A solution to this issue is to compensate for the current in the left arm by application of a higher drift current to arm 1 $I_d^1 > I_d^2 + I_d^3 + I_d^4$ while keeping $I_d^2 - I_d^4$ high enough to

prevent propagation in arms 2–4. This is not very efficient because it would lead to increased power consumption.

E. Geometry IV

Alternatively, the spin current propagating in the left arm can be reduced by change of the carrier density in some selected arms. This allows us to apply all four drift currents in the same direction.

The results for such a device geometry are reported in Fig. 4. In this case, to obtain the most-efficient operation, the charge carriers in the left and top arms are holes, whereas the other parts of the sample are electron doped [see Fig. 4(a)]. We see that in this case there is a substantial increase in the maximum R_s that can be measured in arm

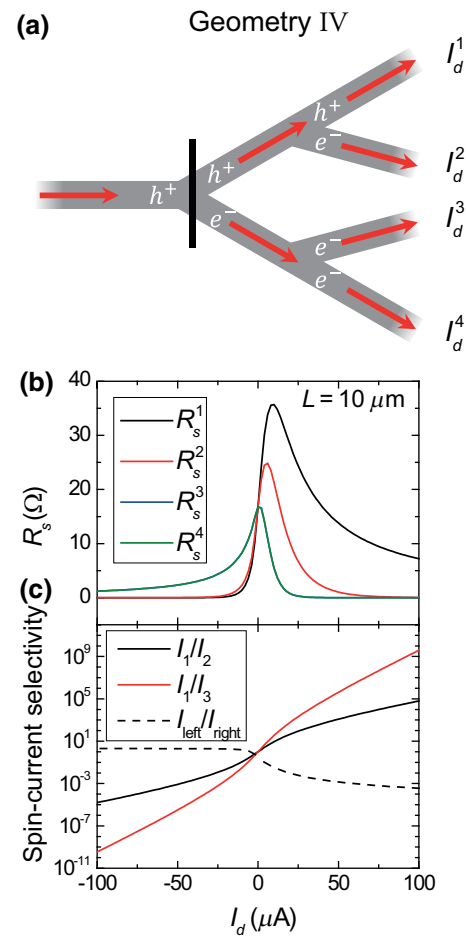


FIG. 4. (a) Device geometry IV, with the spin currents propagating to output 1 for positive I_d in the direction of the red arrows. The carriers are electrons everywhere apart from the top arm, the top and bottom bifurcations are at a distance of $x_1 = 5 \mu\text{m}$ from the spin injector, the detectors are at $L = 10 \mu\text{m}$, and the arms are assumed to be infinitely long. (b) R_s versus I_d in arms 1–4 at L . R_s^3 and R_s^4 are identical over all the range. (c) Spin-current selectivity between arm 1 and arm 2 and between arm 1 and arm 3 calculated at $x = L$, and $I_{\text{left}}/I_{\text{right}}$ calculated at $x = 0$.

TABLE III. Performance for device geometries I–IV. The on:off ratio is defined as $I_{\text{top}}/I_{\text{bot}}$ for geometries I and II. In the case of geometries III and IV, the on:off ratio is defined as I_1/I_2 (I_1/I_3).

	Geometry I		Geometry II		Geometry III		Geometry IV	
I_d (μA)	20	100	20	100	26	100	26	100
On:off ratio	127	1.1×10^7	127	1.1×10^7	99 (614)	6.2×10^4 (3.1×10^8)	$99 (2.6 \times 10^3)$	$6.2 \times 10^4 (3.9 \times 10^9)$
$I_{\text{left}}/I_{\text{right}}$	0.23	0.1	3.1×10^{-2}	1.4×10^{-3}	4.1	12	5.4×10^{-3}	3.5×10^{-4}

1 for positive I_d . In this situation, most of the spins propagate toward the top arm with spin-current selectivities up to 5.4×10^4 between arm 1 and arm 2 and 3.9×10^9 between arm 1 and arm 3. Additionally, the spin currents propagating to the left are 3.5×10^{-3} times smaller than the ones propagating to the right. This efficiency is provided by the drift current, which is $4 \times I_d$ and opposes propagation to the left arm. We also note that in this case there is drift in all the arms and, as a consequence, propagation does not rely on slow diffusion. This can be beneficial for the device performance since it enables faster operations.

We are also interested in the device performance at lower drift currents. In particular, for $I_d = 26 \mu\text{A}$, $I_1/I_2 = 99$, $I_1/I_3 = 2.6 \times 10^3$, and $I_{\text{left}}/I_{\text{right}} = 5.4 \times 10^{-3}$ which we believe should suffice for practical purposes.

IV. DISCUSSION

A. Comparison with other approaches

As mentioned above, there are other methods to control the spin currents in graphene. Lin *et al.* [14] showed that, due to the change of the spin-transport parameters with the carrier density, one can realize demultiplexer functionality in a Y-shaped device with local gates addressing each arm individually. This approach has two drawbacks with respect to our approach. Firstly, spin transport in this case is of diffusive nature and, therefore, operation is slower as compared with that in drift-based devices. Secondly, tuning the local gates gives substantially smaller contrast between *on* and *off* states as compared with the drift case. This is caused by the relatively low tunability of spin-transport parameters in graphene.

Another possibility is to control spin absorption from graphene to an adjacent TMD material [12]. On:off ratios up to 60 have been demonstrated experimentally and can be further increased in high-quality devices. However, implementation of this technique for demultiplexer operations, which relies on slow diffusive transport, would result in an overall major suppression of the spin signal that reaches the targeted arm. This is caused by the proximity-induced spin-orbit coupling in the graphene channel [33,34] that reduces the spin lifetime. Consequently, this approach leads to reduced spin relaxation lengths that require an increase of the input power to achieve signals of the same magnitude.

B. Multiplexer operation and device optimization

For geometries I and II the use of drift also allows multiplexer operation. This can be achieved by placement of two spin injectors on the right side in the sketches in Fig. 1a and 2(a) at a distance significantly longer than the upstream spin relaxation length λ_+ . The modulation of the spin relaxation length induced by drift enables one to select the input that will determine the spin current at the bifurcation point.

The main limitation of the drift approach for spin-based demultiplexer and multiplexer operations is the power consumption, which is caused by the drift currents applied in the channel. We suggest two different ways to overcome this issue. The first approach is to increase the distance at which the detectors are placed. This results in higher contrast between *on* and *off* states for lower drift currents. However, this approach also results in lower spin signals and currents because relaxation occurring in the channel reduces the spin accumulation in an exponential way.

Since the drift velocity is inversely proportional to the carrier density, reduction of this parameter leads to higher power efficiencies. This can be achieved by use of semiconducting channels [35,36]. In particular, black phosphorus is a 2D semiconductor in which spin lifetimes in the nanosecond range have been reported up to room temperature [37]. Such lifetimes, together with its high electronic mobilities [38] and drift-velocity saturations of up to 1.2×10^5 m/s at room temperature [39], make black phosphorus a promising material for spin-drift-based devices.

V. CONCLUSIONS

In conclusion, we show that by applying a drift current to a Y-shaped graphene-based device spin currents can be directed in a highly efficient way (see Table III), allowing a practical realization of a simple spin-based demultiplexer. In particular, for a drift-current density of $20 \mu\text{A}/\mu\text{m}$, spin-current selectivities up to 10^2 can be achieved in a 10- μm -long device. We also perform calculations for a device geometry that consists of two Y-shaped graphene channels connected to the outputs of another Y-shaped device, mimicking a demultiplexer with one input and four outputs, and find that a similar performance can be achieved when a drift-current density of $25 \mu\text{A}/\mu\text{m}$ is applied. We also explain how the effect of drift can be

used to achieve multiplexer operation and argue that the introduction of drift is favorable to increase the device operation speed. We believe this is a relevant step forward toward a new generation of spintronic devices with different functionalities.

ACKNOWLEDGMENTS

We acknowledge T.J. Schouten, H.M. de Roos, H. Adema, and J.G. Holstein for technical assistance and J.C. Leutenantsmeyer, T.S. Ghiasi, and J. Peiro for discussions. The research leading to these results received funding from the People Programme (Marie Curie Actions) of the European Union's Seventh Framework Programme FP7/2007–2013 under REA grant agreement no. 607904-13 (Spinograph), the European Union's Horizon 2020 research and innovation programme under grant agreements no. 696656 and no. 785219 (Graphene Flagship Core 1 and Core 2), NanoNed, the Zernike Institute for Advanced Materials, and the Spinoza Prize awarded to B.J.vW. by the Netherlands Organization for Scientific Research.

-
- [1] J. Fabian, A. Matos-Abiague, C. Ertler, P. Stano, and I. Zutic, Semiconductor spintronics, *Acta Phys. Slovaca* **57**, 565 (2007).
- [2] A. H. Castro Neto, F. Guinea, N. M. R. Peres, K. S. Novoselov, and A. K. Geim, The electronic properties of graphene, *Rev. Mod. Phys.* **81**, 109 (2009).
- [3] Nikolaos Tombros, Csaba Jozsa, Mihaita Popinciuc, Harry T. Jonkman, and Bart J. Van Wees, Electronic spin transport and spin precession in single graphene layers at room temperature, *Nature* **448**, 571 (2007).
- [4] Wei Han, Roland K. Kawakami, Martin Gmitra, and Jaroslav Fabian, Graphene spintronics, *Nat. Nanotechnol.* **9**, 794 (2014).
- [5] Stephan Roche, Johan Akerman, Bernd Beschoten, Jean-Christophe Charlier, Mairbek Chshiev, Saroj Prasad Dash, Bruno Dlubak, Jaroslav Fabian, Albert Fert, Marcos Guimarães, Francisco Guinea, Irina Grigorieva, Christian Schönenberger, Pierre Seneor, Christoph Stampfer, Sergio O. Valenzuela, Xavier Waintal, and Bart J. van Wees, Graphene spintronics: The European flagship perspective, *2D Mater.* **2**, 030202 (2015).
- [6] Marc Drögel, Christopher Franzen, Frank Volmer, Tobias Pohlmann, Luca Banszerus, Maik Wolter, Kenji Watanabe, Takashi Taniguchi, Christoph Stampfer, and Bernd Beschoten, Spin lifetimes exceeding 12 ns in graphene nonlocal spin valve devices, *Nano Lett.* **16**, 3533 (2016).
- [7] Josep Inglà-Aynés, Rick J. Meijerink, and Bart J. van Wees, Eighty-eight percent directional guiding of spin currents with 90 μm relaxation length in bilayer graphene using carrier drift, *Nano Lett.* **16**, 4825 (2016).
- [8] Mallikarjuna Gurram, Siddhartha Omar, and Bart J. van Wees, Bias induced up to 100% spin-injection and detection polarizations in ferromagnet/bilayer-hBN/graphene/hBN heterostructures, *Nat. Commun.* **8**, 248 (2017).
- [9] Simranjeet Singh, Jyoti Katoch, Tiancong Zhu, Ryan J. Wu, Adam S. Ahmed, Walid Amamou, Dongying Wang, K. Andre Mkhoyan, and Roland K. Kawakami, Strontium oxide tunnel barriers for high quality spin transport and large spin accumulation in graphene, *Nano Lett.* **17**, 7578 (2017).
- [10] Ingmar Neumann, Marius V. Costache, Germà Bridoux, Juan F. Sierra, and Sergio O. Valenzuela, Enhanced spin accumulation at room temperature in graphene spin valves with amorphous carbon interfacial layers, *Appl. Phys. Lett.* **103**, 112401 (2013).
- [11] Hua Wen, Hanan Dery, Walid Amamou, Tiancong Zhu, Zhisheng Lin, Jing Shi, Igor Zutić, Ilya Krivorotov, Lu J. Sham, and Roland K. Kawakami, Experimental demonstration of XOR operation in graphene magnetologic gates at room temperature, *Phys. Rev. Appl.* **5**, 044003 (2016).
- [12] Wenjing Yan, Oihana Txoperena, Roger Llopis, Hanan Dery, Luis E. Hueso, and Felix Casanova, A two-dimensional spin field-effect switch, *Nat. Commun.* **7**, 13372 (2016).
- [13] André Dankert and Saroj P. Dash, Electrical gate control of spin current in van der Waals heterostructures at room temperature, *Nat. Commun.* **8**, 16093 (2017).
- [14] Xiaoyang Lin, Li Su, Zhizhong Si, Youguang Zhang, Arnaud Bournel, Yue Zhang, Jacques-Olivier Klein, Albert Fert, and Weisheng Zhao, Gate-driven pure spin current in graphene, *Phys. Rev. Appl.* **8**, 034006 (2017).
- [15] T.-Y. Yang, J. Balakrishnan, F. Volmer, A. Avsar, M. Jaiswal, J. Samm, S. R. Ali, A. Pachoud, M. Zeng, and M. Popinciuc *et al.*, Observation of long spin-relaxation times in bilayer graphene at room temperature, *Phys. Rev. Lett.* **107**, 047206 (2011).
- [16] Wei Han and Roland K. Kawakami, Spin relaxation in single-layer and bilayer graphene, *Phys. Rev. Lett.* **107**, 047207 (2011).
- [17] Ahmet Avsar, Tsung-Yeh Yang, Sukang Bae, Jayakumar Balakrishnan, Frank Volmer, Manu Jaiswal, Zheng Yi, SyedRizwan Ali, Gernot Güntherodt, Byung Hee Hong, Bernd Beschoten, and Barbaros Özyilmaz, Toward wafer scale fabrication of graphene based spin valve devices, *Nano Lett.* **11**, 2363 (2011).
- [18] C. Józsa, M. Popinciuc, N. Tombros, H. T. Jonkman, and B. J. Van Wees, Electronic spin drift in graphene field-effect transistors, *Phys. Rev. Lett.* **100**, 236603 (2008).
- [19] Béla G. Lipták, *Instrument Engineers' Handbook* (CRC Press, Boca Raton, Florida, 2002), 3rd ed., Vol. 3, p. 343.
- [20] Tamara Dean, *Network+ Guide to Networks* (Cengage Learning, Boston, 2010), p. 82.
- [21] B. Govindarajalu, *IBM PC and Clones* (Tata McGraw-Hill, New York, 2008), p. 198.
- [22] Behtash Behin-Aein, Deepanjan Datta, Sayeef Salahuddin, and Supriyo Datta, Proposal for an all-spin logic device with built-in memory, *Nat. Nanotechnol.* **5**, 266 (2010).
- [23] Behtash Behin-Aein, Angik Sarkar, Srikant Srinivasan, and Supriyo Datta, Switching energy-delay of all spin logic devices, *Appl. Phys. Lett.* **98**, 123510 (2011).
- [24] Z. G. Yu and M. E. Flatté, Spin diffusion and injection in semiconductor structures: Electric field effects, *Phys. Rev. B* **66**, 235302 (2002).

- [25] M. Popinciuc, C. Józsa, P. J. Zomer, N. Tombros, A. Veligura, H. T. Jonkman, and B. J. Van Wees, Electronic spin transport in graphene field-effect transistors, *Phys. Rev. B* **80**, 214427 (2009).
- [26] The spin current is defined as $I_s = I_\uparrow - I_\downarrow$, where I_\uparrow is the current of up spins and I_\downarrow is the current of down spins.
- [27] I. J. Vera-Marun, V. Ranjan, and B. J. van Wees, Nonlinear interaction of spin and charge currents in graphene, *Phys. Rev. B* **84**, 241408 (2011).
- [28] Marcos H. D. Guimarães, A. Veligura, P. J. Zomer, T. Maassen, I. J. Vera-Marun, N. Tombros, and B. J. van Wees, Spin transport in high-quality suspended graphene devices, *Nano Lett.* **12**, 3512 (2012).
- [29] Jens Martin, N. Akerman, G. Ulbricht, T. Lohmann, J. H. v Smet, K. Von Klitzing, and Amir Yacoby, Observation of electron-hole puddles in graphene using a scanning single-electron transistor, *Nat. Phys.* **4**, 144 (2008).
- [30] Alexander S. Mayorov, Daniel C. Elias, Ivan S. Mukhin, Sergey V. Morozov, Leonid A. Ponomarenko, Kostya S. Novoselov, A. K. Geim, and Roman V. Gorbachev, How close can one approach the dirac point in graphene experimentally? *Nano Lett.* **12**, 4629 (2012).
- [31] Megan A. Yamoah, Wenmin Yang, Eric Pop, and David Goldhaber-Gordon, High-velocity saturation in graphene encapsulated by hexagonal boron nitride, *ACS Nano* **11**, 9914 (2017).
- [32] Correction for the saturation in v_d leads to a drift velocity of 7.4×10^4 m/s, a correction of only 7.5%. For the highest drift current reported here, $I_d = 400 \mu\text{A}/\mu\text{m}$, $v_d = 3.2 \times 10^5$ m/s, which after correction becomes 2.3×10^5 m/s, a correction of 28%.
- [33] Talieh S. Ghiasi, Josep Ingla-Aynés, Alexey A. Kaverzin, and Bart J. van Wees, Large proximity-induced spin lifetime anisotropy in transition-metal dichalcogenide/graphene heterostructures, *Nano Lett.* **17**, 7528 (2017).
- [34] L. Antonio Bentlaz, Juan F. Sierra, Williams Savero Torres, and Sergio O. Valenzuela, Strongly anisotropic spin relaxation in graphene-transition metal dichalcogenide heterostructures at room temperature, *Nat. Phys.* **14**, 303 (2018).
- [35] J. M. Kikkawa and D. D. Awschalom, Lateral drag of spin coherence in gallium arsenide, *Nature* **397**, 139 (1999).
- [36] Ian Appelbaum, Biqin Huang, and Douwe J. Monsma, Electronic measurement and control of spin transport in silicon, *Nature* **447**, 295 (2007).
- [37] Ahmet Avsar, Jun Y. Tan, Marcin Kurpas, Martin Gmitra, Kenji Watanabe, Takashi Taniguchi, Jaroslav Fabian, and Barbaros zyilmaz, Gate-tunable black phosphorus spin valve with nanosecond spin lifetimes, *Nat. Phys.* **13**, 888 (2017).
- [38] Ahmet Avsar, Jun Y. Tan, Xin Luo, Khoong Hong Khoo, Yuting Yeo, Kenji Watanabe, Takashi Taniguchi, Su Ying Quek, and Barbaros zyilmaz, van der Waals bonded co/h-BN contacts to ultrathin black phosphorus devices, *Nano Lett.* **17**, 5361 (2017).
- [39] Xiaolong Chen, Chen Chen, Adi Levi, Lothar Houben, Bingchen Deng, Shaofan Yuan, Chao Ma, Kenji Watanabe, Takashi Taniguchi, Doron Naveh, Xu Du, and Fengnian Xia, Large-velocity saturation in thin-film black phosphorus transistors, *ACS Nano* **12**, 5003 (2018).